J Membrane Biol (2008) 222:151–166
DOI 10.1007/s00232-008-9113-9

Contribution of L-Type Ca^{2+} Channels to Early Afterdepolarizations Induced by I_{Kr} and I_{Ks} Channel Suppression in Guinea Pig Ventricular Myocytes

Mitsuhiko Yamada · Keisuke Ohta · Atsunori Niwa · Natsuko Tsujino · Tsutomu Nakada · Masamichi Hirose

Received: 21 February 2008 / Accepted: 16 May 2008 / Published online: 20 June 2008

Abstract Early afterdepolizations (EADs) induced by suppression of cardiac delayed rectifier I_{Kr} and/or I_{Ks} channels cause fatal ventricular tachyarrhythmias. In guinea pig ventricular myocytes, partial block of one of the channels with complete block of the other reproducibly induced EADs. Complete block of both I_{Kr} and I_{Ks} channels depolarized the take-off potential and reduced the amplitude of EADs, which in some cases were not clearly separated from the preceding action potentials. A selective L-type Ca^{2+} ($I_{Ca,L}$) channel blocker, nifedipine, effectively suppressed EADs at submicromolar concentrations. As examined with the action potential-clamp method, $I_{Ca,L}$ channels mediated inward currents with a spike and dome shape during action potentials. $I_{Ca,L}$ currents decayed mainly due to inactivation in phase 2 and deactivation in phase 3 repolarization. When EADs were induced by complete block of I_{Kr} channels with partial block of I_{Ks} channels, repolarization of the action potential prior to EAD take-off failed to increase I_{K1} currents and thus failed to completely deactivate $I_{Ca,L}$ channels, which reactivated and mediated inward currents during EADs. When both I_{Kr} and I_{Ks} channels were completely blocked, $I_{Ca,L}$ channels were not deactivated and mediated sustained inward currents until the end of EADs. Under this condition, the recovery and reactivation of $I_{Ca,L}$ channels were absent before EADs. Therefore, an essential mechanism underlying EADs caused by suppression of the delayed rectifiers is the failure to completely deactivate $I_{Ca,L}$ channels.

M. Yamada (✉) · K. Ohta · A. Niwa · N. Tsujino · T. Nakada · M. Hirose
Department of Molecular Pharmacology, Shinshu University School of Medicine, 3-1-1 Asahi, Matsumoto, Nagano 390-8621, Japan
e-mail: myamada@shinshu-u.ac.jp

Keywords Early afterdepolarization · I_{Kr} channel · I_{Ks} channel · L-type Ca^{2+} channel · Long QT syndrome · Action potential clamp · Cardiac electrophysiology

Introduction

The voltage-dependent L-type Ca^{2+} ($I_{Ca,L}$) channel is the main source of Ca^{2+} entry during an action potential in cardiac myocytes (McDonald et al. 1994). During an action potential, an $I_{Ca,L}$ current shows the form of a spike followed by a dome (Doerr et al. 1990; Arreola et al. 1991; Grantham and Cannell 1996; Linz and Myer 1998a 2000). The initial spike causes Ca^{2+} release from the sarcoplasmic reticulum, whereas the following slow dome component reloads the sarcoplasmic reticulum (Fabiato 1985; Linz and Myer 1998b). The form of $I_{Ca,L}$ currents during action potentials is finely tuned by inactivation, deactivation and alterations in the driving force (Luo and Rudy 1994; Linz and Myer 1998a). Inactivation of cardiac $I_{Ca,L}$ channels is both voltage- and Ca^{2+}-dependent (Kass and Sanguinetti 1984; Lee et al. 1985). Impairment of either type of inactivation results in prominent prolongation of cardiac action potentials (Alseikhan et al. 2002; Splawski et al. 2004), indicating that $I_{Ca,L}$ channels play a significant role in determining cardiac action potential duration.

Long QT (LQT) syndrome describes a group of disorders that is usually characterized by a prolonged QT interval on the electrocardiogram (Keating and Sanguinetti 2001). It is associated with syncope and sudden death due to episodic cardiac arrhythmias. Among the eight types of congenital LQT syndrome, LQT1 is the most frequent, caused by impairment of the slow component of delayed rectifier K^+ current (I_{Ks}). A more common acquired LQT syndrome can arise from suppression of the rapid

component of delayed rectifier K^+ current (I_{Kr}) by various factors including drugs.

In LQT syndromes, the action potentials of ventricular myocytes are prolonged and may be associated with early afterdepolarizations (EADs). EADs are defined as depolarizing afterpotentials that interrupt or delay normal repolarization of cardiac action potentials (Cranefield and Aronson 1988). Depending on the membrane potential at which EADs take off, they are classified into two categories: low-membrane potential (or phase 2) EADs that occur during phase 2 repolarization and high-membrane potential (or phase 3) EADs that occur during phase 3 repolarization (Damiano and Rose 1984). The former arise from the reduction of net outward currents during phase 2 repolarization, which occurs in LQT syndromes (Brugada and Wellens 1985; Antzelevitch and Shimizu 2002; Splawski et al. 2004).

It has been suggested that when delayed rectifier K^+ currents are reduced an $I_{Ca,L}$ channel causes phase 2 EADs (Marbán et al. 1986; Anderson et al. 1998; Zeng and Rudy 1995). January and Riddle (1989) found that the $I_{Ca,L}$ channel agonist BayK8644 caused EADs to take off at ~ -30 mV and to have an amplitude of up to ~ 40 mV in sheep Purkinje fibers; they concluded that $I_{Ca,L}$ channels recovered before EADs and generated EADs. This mechanism is also suggested to underlie EADs caused by suppression of K^+ currents by a theoretical study (Zeng and Rudy 1995). However, this notion has not been experimentally tested.

In this study of isolated guinea pig ventricular myocytes, we found that when I_{Kr} and I_{Ks} channels were suppressed, EADs took off from a more depolarized potential (~ -10–0 mV) and had a much smaller amplitude (<15 mV) than January and Riddle (1989) found. Under this condition, the recovery of $I_{Ca,L}$ channels before EADs was modest, if any, and EADs arose mainly from the failure to deactivate $I_{Ca,L}$ channels and the resulting sustained inward current at the end of phase 2 repolarization.

Methods

Isolation of Cardiac Myocytes

Ventricular myocytes were enzymatically isolated from the hearts of male guinea pigs (300–600 g) as previously described (Yamada et al. 1993). Briefly, the animals were killed with intraperitoneal injection of 50–200 mg of pentobarbital. The hearts were quickly removed and retrogradely perfused in a Langendorff apparatus with 400 ml of modified Tyrode solution (for composition, see below) and then with 100 ml of nominally Ca^{2+}-free Tyrode solution (for composition, see below) at 37°C. Thereafter, the hearts were digested with nominally Ca^{2+}-free Tyrode solution containing 0.3 mg/ml collagenase at 37°C for 55 min. The reaction was terminated with perfusion of 50 ml KB solution (for composition, see below). The digested hearts were stored in KB solution at 4°C for up to 6 h before use. Ventricular myocytes were isolated by gently shaking a small piece of the ventricular myocardium in a recording chamber filled with the modified Tyrode solution. All experiments were carried out in accordance with the "Guidelines for Animal Experimentation" of Shinshu University.

Electrophysiology

Membrane voltage and currents were recorded with a patch-clamp amplifier (Axopatch 200B; Molecular Devices, Sunnyvale, CA) in the whole-cell configuration of the patch-clamp method (Hamill et al. 1981). In all experiments, data acquisition was done with an in-house computer program. Patch pipettes were fabricated from borosilicate glass capillaries (Kimax-51; Kimble Glass, Vineland, NJ) and had a resistance of ≤ 2 MΩ when filled with pipette solution (for composition, see below). The pipette offset potential, series resistance and cell capacitance were compensated with the amplifier. The series resistance and membrane capacitance compensation were repeatedly adjusted every 2–3 min during experiments and were 3.7 ± 0.1 MΩ and 170.7 ± 4.1 pF at the end of experiments, respectively ($n = 239$). A leak current was not subtracted. All experiments were done in modified Tyrode solution at 35–37°C unless otherwise indicated.

In current-clamp experiments, action potentials were elicited with a rectangular current pulse of 1–4 nA and 2 ms duration at 0.33 Hz. Recorded action potentials were low-pass filtered at 2 kHz (−3 dB), digitized at 5 kHz and stored on the hard disk of a computer. In some experiments, E4031, chromanol 293B (293B), nifedipine and/or SEA0400 were used to block, respectively, I_{Kr}, I_{Ks} and $I_{Ca,L}$ channels and Na^+–Ca^{2+} exchange.

It has been reported that there are M cells in the guinea pig ventricle (Sicouri et al. 1996). Compared with other ventricular myocytes, M cells show a disproportionate prolongation of their action potentials in response to either slowing of the stimulation rate or application of class III antiarrhythmic drugs. In our hands, however, it was difficult to reliably and reproducibly isolate M cells from the digested whole ventricle. In addition, we did not find any cells where E4031 (10 μM) alone significantly prolonged action potential duration or caused EADs (Fig. 1). Thus, we did not distinguish M cells from other myocardial cells in this study.

Action potential-clamp experiments were conducted following the protocols outlined by Linz and Meyer (1998a). Four action potentials representing different

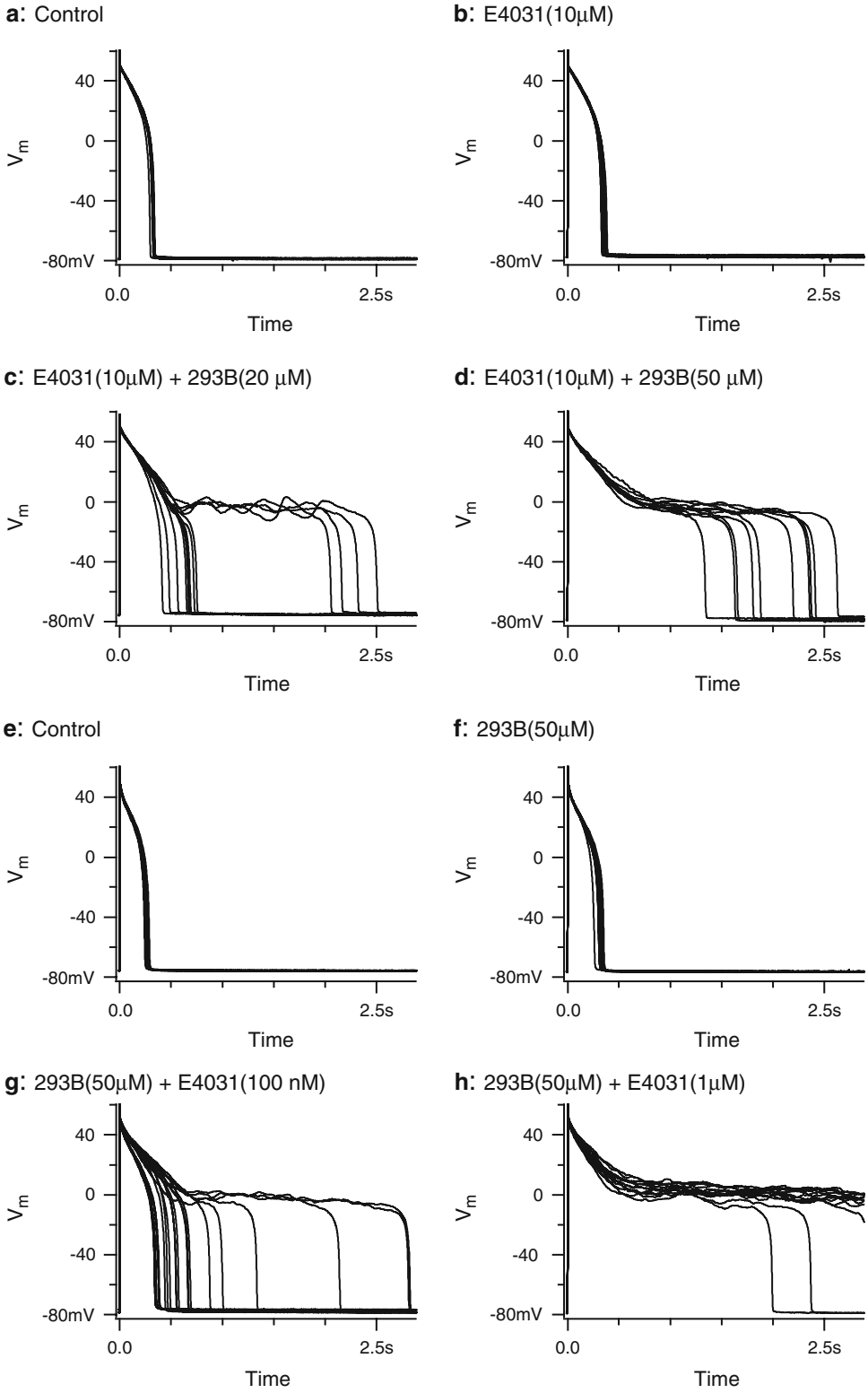

Fig. 1 Effects of E4031 and chromanol 293B on the action potentials of isolated guinea pig ventricular myocytes. Isolated guinea pig ventricular myocytes were paced at 0.33 Hz under the experimental conditions indicated with each trace. (**a–d**) and (**e–h**) show representative traces recorded from two different myocytes. In each case, between 10 and 20 consecutively recorded action potentials in the steady state are superimposed. In (**h**), most of the action potentials were longer than the time span of the graph. 293B indicates chromanol 293B

experimental conditions were recorded under current-clamp, DA-converted and subsequently used as voltage command pulses (Figs. 3–6). Each action potential stimulus was preceded by a 200-ms rectangular pulse to −40 m*V* to inactivate voltage-dependent Na^+ channels and T-type Ca^{2+} channels (Linz and Myer 1998a). The holding potential was −80 m*V*. Each action potential stimulus was applied to myocytes at 0.33 Hz.

An $I_{Ca,L}$ current was isolated as the membrane current that was inhibited by addition of 100 μM Cd^{2+} and 10 μM nifedipine. Nifedipine (10 μM) alone did not completely suppress the initial part of $I_{Ca,L}$ currents, while Cd^{2+} (100 μM) failed to completely suppress the late phase of $I_{Ca,L}$ currents in action potentials. I_{Kr} and I_{Ks} currents were, respectively, isolated as E4031- (10 μM) or 293B- (50 μM) sensitive difference currents. An I_{K1} current was isolated as the Ba^{2+}- (2 mM) sensitive difference current. To isolate each membrane current during action potential stimuli, these drugs were added sequentially in this order in a cumulative manner.

The steady-state activation of $I_{Ca,L}$ channels (d_∞) was estimated with conventional rectangular voltage-clamp steps. In these experiments, the membrane potential was depolarized from −80 to −40 mV for 200 ms and then for 500 ms to potentials between −40 and +70 mV with a 5-mV increment every 3 s. The peak amplitude of $I_{Ca,L}$ currents evoked by the 500-ms test pulse was normalized to the membrane capacitance and plotted against membrane voltage. The peak current density–voltage relationship was fitted with the following equation:

$$I = g_{Ca,L}(1/\{1 + \mathrm{Exp}[(V_{0.5} - V_m)/k]\})(V_m - E_{Ca}) \quad (1)$$

where I is the peak $I_{Ca,L}$ density, $g_{Ca,L}$ is the maximum conductance density of $I_{Ca,L}$ channels, $V_{0.5}$ is the membrane potential at which $d_\infty = 0.5$, V_m is the membrane potential, k is the slope factor and E_{Ca} is the apparent reversal potential of $I_{Ca,L}$ channels. The best fit of this equation to the data was obtained with $g_{Ca,L} = 181$ pS/pF, $V_{0.5} = 13.9$ mV, $k = 5.13$ mV and $E_{Ca} = +57.8$ mV. From these parameters, d_∞ was calculated from the following equation:

$$d_\infty = 1/\{1 + \mathrm{Exp}[(V_{0.5} - V_m)/k]\} \quad (2)$$

Then, the activation of $I_{Ca,L}$ channels during action potentials (d_{AP}) was calculated from equation 2 and the time-dependent change in V_m, except for the initial 4 ms. This assumes that the activation kinetics of $I_{Ca,L}$ channels are sufficiently fast compared with the time-dependent change in V_m (Linz and Myer 2000).

Inactivation of $I_{Ca,L}$ channels during action potentials (f_{AP}) was assessed with a gapped double pulse protocol (Linz and Myer 1998a). In this protocol, the membrane potential was first depolarized from the resting membrane potential (∼−80 mV) to −40 mV for 200 ms and then an action potential waveform was applied (P1). The action potential was interrupted at different times and voltage values with a voltage step to −40 mV for 5 ms followed by a 200-ms test pulse to +10 mV (P2). f_{AP} was assessed by normalizing the amplitude of $I_{Ca,L}$ currents during P2 in the presence of P1 relative to that which had been recorded in the absence of P1.

Inactivation of $I_{Ca,L}$ channels is both voltage- and Ca^{2+}-dependent (Kass and Sanguinetti 1984; Lee et al. 1985). Total f_{AP} was assessed as above in solution containing 1.8 mM Ca^{2+}. The voltage-dependent component of inactivation in action potentials (f_{AP_V}) was assessed in solution containing 1.8 mM Ba^{2+} instead of Ca^{2+} (Kass and Sanguinetti 1984; Lee et al. 1985). The Ca^{2+}-dependent component of inactivation in action potentials (f_{AP_Ca}) was calculated with equation 3, assuming that voltage- and Ca^{2+}-dependent inactivation occur through independent mechanisms (Hardley and Lederer 1991; Linz and Myer 1998a; Shirokov et al. 1993).

$$f_{AP} = f_{AP\_V} f_{AP\_Ca} \quad (3)$$

Data Analysis

Recorded cell currents were low-pass filtered at 10 kHz (−3 dB), digitized at 47.2 kHz with a PCM converter system (VR-10B; Instrutech, New York, NY) and recorded on videocassette tapes. For off-line analysis, data were reproduced, low-pass filtered at 2 kHz (−3 dB), digitized at 5 kHz with an AD converter (ITC16I, Instrutech) and analyzed with Patch Analyst Pro (MT Corp., Hyogo, Japan).

Solutions and Chemicals

The modified Tyrode solution contained (in mM) 136.5 NaCl, 5.4 KCl, 1.8 $CaCl_2$, 0.53 $MgCl_2$, 5.5 glucose and 5.5 HEPES (pH adjusted to 7.4 with NaOH). $CaCl_2$ was omitted from the nominally Ca^{2+}-free Tyrode solution. In some experiments, 1.8 mM $BaCl_2$ replaced 1.8 mM $CaCl_2$. The KB solution contained (in mM) 10 taurine, 10 oxalic acid, 70 L-glutamic acid, 25 KCl, 10 KH_2PO_4, 11 glucose, 0.5 EGTA and 10 HEPES (pH was adjusted 7.3 with KOH). The pipette solution contained (in mM) 120 K D-glutamate, 20 KCl, 10 NaCl, 5 $MgCl_2$, 0.1 EGTA, 3 ATP and 5 HEPES (pH was adjusted to 7.4 with KOH). Stock solutions of nifedipine, 293B and SEA0400 were prepared in 100% dimethyl sulfoxides (DMSO) at 10, 50 and 10 mM, respectively. Final dilutions were in the modified Tyrode solution. The maximum final concentration of DMSO (0.1%) did not affect membrane currents.

SEA0400 was provided by Taisho Pharmaceutical (Tokyo, Japan). Pentobarbital sodium was purchased from Abbott Laboratories (North Chicago, IL). Collagenase was from Worthington Biochemical (type II; Freehold, NJ). Nifedipine and E4031 were from Wako Pure Chemical Industries (Osaka, Japan). 293B was from Sigma-Aldrich (St. Louis, MO). All other chemicals were purchased from Wako Pure Chemical Industries.

Statistical Analysis

Data are shown as mean ± standard error (SE). Statistical differences were evaluated with Student's paired or unpaired *t*-test. $P < 0.05$ was considered significant.

Results

EADs Can Be Induced by I_{Kr} and I_{Ks} Blockers

Figure 1 shows the induction of EADs in action potentials by blockade of different K^+ currents. Action potentials were induced by pacing isolated myocytes at 0.33 Hz in the presence or absence of different concentrations of the I_{Kr} blocker E4031 and the I_{Ks} blocker chromanol 293B (293B) (Sanguinetti and Jurkiewicz 1990; Bosch et al. 1998). This pacing frequency was chosen since EADs tend to occur at bradycardia (Cranefield and Aronson 1988). Compared with the control (Fig. 1a), 10 μM E4031 alone only slightly prolonged action potential duration and did not induce EADs (Fig. 1b). The further addition of 20 μM 293B strongly prolonged action potential duration and induced EADs (Fig. 1c). EADs arose when action potential repolarization reached −8 to 0 m*V*; they were sustained for as long as ∼2 s, and they had an amplitude of 2–15 m*V*. When the concentration of 293B was increased to 50 μM, a diminished amplitude (∼2 m*V*) of EADs occurred from a more depolarized take-off potential (∼0 m*V*) (Fig. 1d). Similar results were obtained in nine other myocytes.

In another myocyte, 50 μM 293B alone only slightly prolonged action potential duration (Fig. 1f) compared with control (Fig. 1e). However, addition of 100 nM E4031 significantly prolonged action potential duration and induced EADs (Fig. 1g). Here, EADs arose when action potential repolarization reached ∼−4 to 0 m*V*; they were sustained for 1–2 s and had an amplitude of 2–3 m*V*. Increasing the concentration of E4031 to 1 μM even further prolonged action potential duration and induced EADs, which were sustained for more than 2.5 s (Fig. 1h). Similar results were obtained in nine other myocytes.

Thus, blockade of either I_{Kr} or I_{Ks} channels alone was not sufficient to prolong action potential duration or induce EADs in isolated guinea pig ventricular myocytes. However, partial blockade of one in the presence of complete blockade of the other strongly prolonged action potential duration and induced EADs. Complete blockade of both I_{Kr} and I_{Ks} channels depolarized the take-off potential and diminished the amplitude of EADs, which in some cases could not be clearly separated from the preceding action potential. We regarded this type of EADs and the prototypical EADs with a clear take-off and depolarization as a continuous spectrum because the latter were gradually transformed to the former as the blockade of I_{Kr} and I_{Ks} channels was progressively strengthened. EADs fused with action potentials did not seem to arise from rundown of inward currents generating EADs because this type of EADs also appeared when 10 μM E4031 and 50 μM 293B were applied soon after formation of the whole-cell configuration (see Fig. 2a).

Effect of Nifedipine on EADs

The upper panel in Fig. 2a shows the effect of nifedipine (10 and 100 nM) on action potentials without EADs under control conditions. Action potentials were elicited by pacing a myocyte at 0.33 Hz. Nifedipine reduced APD_{90} from 448 to 417 (10 nM) and 320 (100 nM) ms. The lower panel in Fig. 2a shows the effect of nifedipine on action potentials with EADs. Action potentials were elicited by pacing a myocyte at 0.33 Hz in the presence of 10 μM E4031 and 50 μM 293B. Nifedipine reduced the duration of 90% repolarization from 1,653 to 1,188 (10 nM) and 591 (100 nM) ms.

Figure 2b shows that nifedipine reduced APD_{90} more potently in the presence of E4031 and 293B than under control conditions. These results indicate that $I_{Ca,L}$ channels may play a more important role in determining the time course of repolarization of action potentials with EADs than those without EADs and, therefore, $I_{Ca,L}$ channels could be critically involved in the genesis and maintenance of EADs.

It has been suggested that Na^+–Ca^{2+} exchanger (I_{Na-Ca}) currents also participate in the genesis of EADs (Priori and Corr 1990; Nagy et al. 2004). Thus, we examined the effect of a selective I_{Na-Ca} blocker, SEA0400, on EADs elicited by 10 μM E4031 and 50 μM 293B. SEA0400 blocks I_{Na-Ca} with a half-maximal inhibitory concentration of 5–100 nM (Matsuda et al. 2001; Birinyi et al. 2005). SEA0400 reduced APD_{90} to 90.4 ± 4.1% (100 nM) and 85.7 ± 6.0% (1 μM) of the control (not shown) ($n = 5$ for each concentration). These effects were much smaller than those of nifedipine (Fig. 2b). Thus, $I_{Ca,L}$ channels seem likely to play a more important role than I_{Na-Ca} in the genesis of EADs when I_{Kr} and I_{Ks} channels are blocked (Zeng and Rudy 1995).

L-Type Ca^{2+} and K^+ Currents Recorded During Guinea Pig Ventricular Action Potentials

We therefore examined the behavior of $I_{Ca,L}$ channels during action potentials. Figure 3 shows total membrane, $I_{Ca,L}$ and K^+ channel currents measured in action potential-clamp experiments. Two different action potential stimuli were used in this analysis (Fig. 3a, b). These action potentials were originally recorded from two different myocytes which had been paced at 0.33 Hz. The action

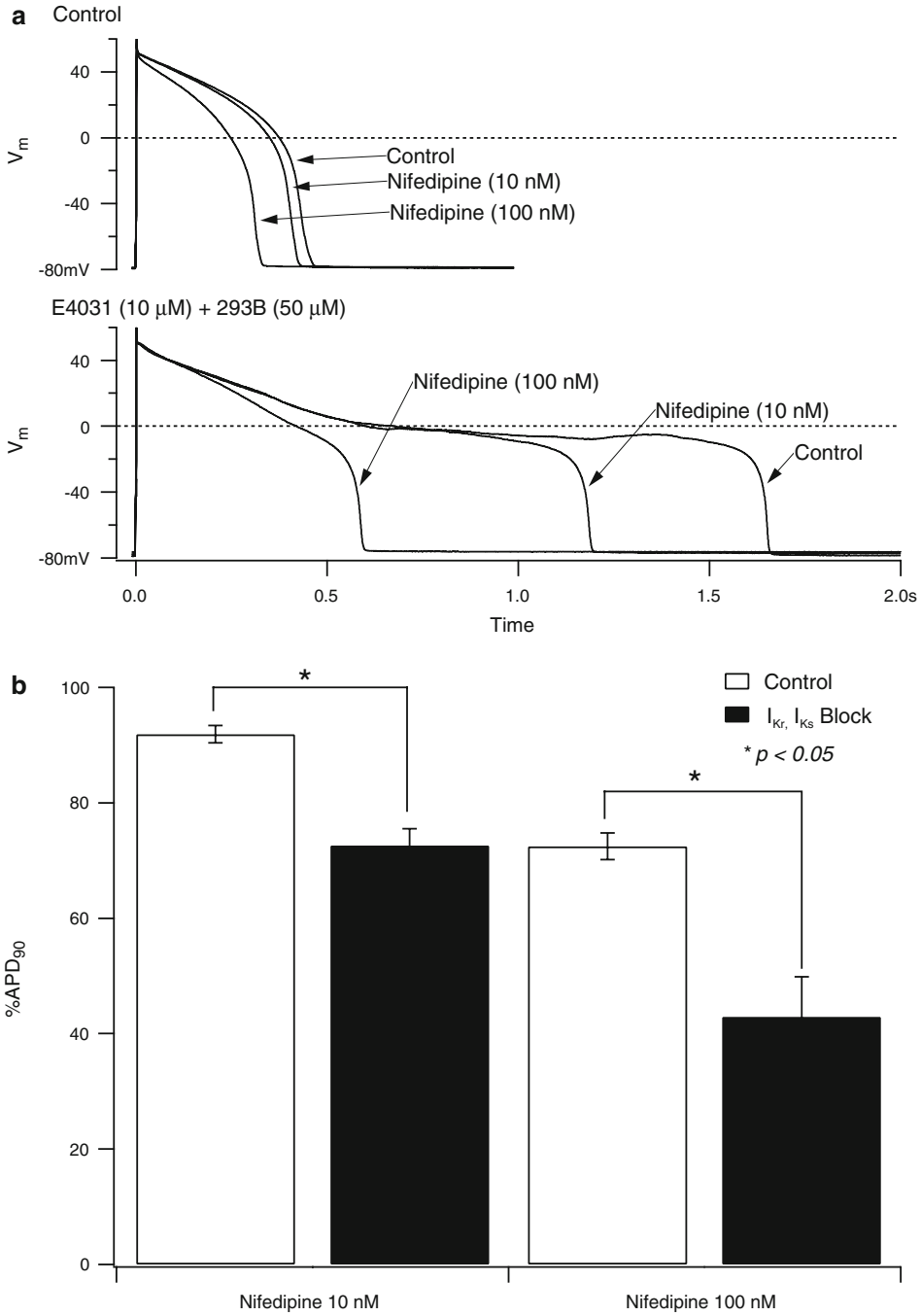

Fig. 2 The effect of nifedipine on action potentials recorded in the presence and absence of E4031 and chromanol 293B. (**a**) Action potentials were recorded by pacing myocytes at 0.33 Hz. In the presence (*below*) and absence (*above*) of 10 μM E4031 and 50 μM 293B, first 10 and then 100 nM nifedipine was applied. (**b**) APD_{90} was measured in the presence of 10 or 100 nM nifedipine and expressed as a percentage of that recorded in the absence of nifedipine. Experiments were done in the absence (*white bars*) and presence (*black bars*) of 10 μM E4031 and 50 μM 293B. Error bars indicate SE of five observations. *Statistically significant difference ($P < 0.05$) as judged by Student's unpaired *t*-test

potential in Fig. 3a was recorded under control conditions, and that shown in 3b was recorded in the presence of 10 μM E4031 and 10 μM 293B. In the following experiments, each action potential stimulus was applied to isolated myocytes at 0.33 Hz.

Figure 3c and d shows the total membrane currents evoked during each action potential. They were outward, increasing gradually during phase 2 repolarization and then rapidly and transiently increased during phase 3 repolarization. The gray trace in Fig. 3d shows that the total membrane current in the presence of 10 μM E4031 and 10 μM 293B was reduced by comparison with the current recorded in control solution (black trace).

An $I_{Ca,L}$ current was isolated as that part of the total membrane current that was inhibited by 100 μM Cd^{2+} and 10 μM nifedipine. In each action potential, an $I_{Ca,L}$ current was always inward with a spike and dome shape (Fig. 3e, f). The peak $I_{Ca,L}$ densities were -3.02 ± 1.43 (Fig. 3e) and -2.14 ± 0.53 (Fig. 3f) pA/pF.

I_{Kr} and I_{Ks} currents were, respectively, isolated as the 10 μM E4031- and 50 μM 293B-sensitive parts of the membrane current. Outward I_{Kr} currents gradually increased

during phase 2 and rapidly decreased in phase 3 of the action potential (Fig. 3g). The I_{Kr} density reached a peak of 0.89 ± 0.07 pA/pF at −29 m*V* (Fig. 3g). The black trace in Fig. 3h illustrates I_{Kr} currents recorded in control solution, which should have been absent when the action potential (Fig. 3b) was recorded in the presence of 10 μM E4031.

I_{Ks} currents initially increased, then decreased gradually during phase 2 repolarization (Fig. 3i, j). They decreased rapidly during phase 3. The gray trace in Fig. 3j illustrates the extent of I_{Ks} inhibition by 10 μM 293B compared to that recorded in control solution (black).

Figure 3k and l shows that inward-rectifier I_{K1} currents were small and outward during phase 2 repolarization of each action potential. In phase 3 repolarization I_{K1} currents first abruptly increased and then decreased as the membrane voltage approached the resting value.

The Kinetics of L-Type Ca^{2+} Channels During Action Potential Clamp

$I_{Ca,L}$ currents in cardiac action potentials can be described in the following extended Hodgkin-Huxley equation (Luo and Rudy 1994; Linz and Myer 1998a, 2000):

$$I_{Ca,L} = g_{Ca,L} d_{AP} f_{AP} (V_m - E_{Ca}) \quad (4)$$

where $I_{Ca,L}$ is I_{CaL} current in an action potential.

The characteristics of activation (d_{AP}) and inactivation (f_{AP}) of I_{CaL} channels during the two different action potential waveforms were dissected. f_{AP} was assessed with the gapped action potential clamp technique (Linz and Myer 1998a). Figure 4a, b illustrates the uninterrupted action potentials. Figure 4c, d illustrates the time-dependent changes in d_{AP}, f_{AP} and f_{AP_V} during each action potential. In each action potential, d_{AP} was almost unity during the peak and phase 2 repolarization and decreased rapidly to zero during phase 3 repolarization. Thus, $I_{Ca,L}$ channels show deactivation during phase 3 repolarization.

The time-dependent change in f_{AP} was measured with 1.8 mM Ca^{2+} in the external solution. In each action potential f_{AP} gradually decreased during phase 2 and increased during phase 3 repolarization (Fig. 4c, d). The time at which f_{AP} was minimal (T_{min}) was 368 (Fig. 4c) and 506 (Fig. 4d) ms. At T_{min}, f_{AP} was 0.085 (Fig. 4c) and 0.071 (Fig. 4d). Thus, $I_{Ca,L}$ channels were not completely inactivated and showed partial recovery during each action potential (Luo and Rudy 1994; Linz and Myer 1998a, 2000).

The voltage-dependent inactivation of $I_{Ca,L}$ channels in action potentials was assessed in the presence of 1.8 mM Ba^{2+} (f_{AP_V} in Fig. 4c, d). Although the values for f_{AP_V} were larger than those for f_{AP} throughout each action potential, they also decreased during phase 2 and increased during phase 3. f_{AP_V} minima were 0.430 at 368 ms (Fig. 4c) and 0.301 at 577 ms (Fig. 4d).

From f_{AP} and f_{AP_V}, the Ca^{2+}-dependent component of inactivation of $I_{Ca,L}$ channels in action potentials (f_{AP_Ca}), a fraction of f_{AP}, was calculated with equation 3 (Fig. 4e, f). In each action potential, f_{AP_Ca} first rapidly and then more gradually decreased during phase 2 repolarization before increasing during phase 3. f_{AP_Ca} minima were 0.198 at 368 ms (Fig. 4e) and 0.220 at 506 ms (Fig. 4h). Values for f_{AP_Ca} were smaller than those for f_{AP_V} throughout phase 2 of each action potential.

These results suggest that Ca^{2+}-dependent inactivation plays a more important role than voltage-dependent inactivation during the first 10 ms and that this is responsible for the initial rapid decay of $I_{Ca,L}$ currents during the action potentials (Fig. 3e, f). This rapid inactivation may mainly result from the release of Ca^{2+} from the sarcoplasmic reticulum (Linz and Myer 1998a). Subsequently, during phase 2 repolarization, both voltage- and Ca^{2+}-dependent inactivation almost equally contributed to the decay of $I_{Ca,L}$ currents. However, $I_{Ca,L}$ channels were incompletely inactivated at T_{min} and then showed recovery. Thus, the decay of $I_{Ca,L}$ currents after T_{min} was due to deactivation (Luo and Rudy 1994; Linz and Myer 1998a, 2000).

K^+ Currents Responsible for Deactivation of L-Type Ca^{2+} Channels During the Action Potential

At T_{min} $I_{Ca,L}$ channels still mediate substantial inward currents because, although f_{AP} is small, d_{AP} and ($V_m - E_{Ca}$) are large (equation 4; Figs. 3e, f and 4c, d). The $I_{Ca,L}$ currents remaining at T_{min} must be eliminated by deactivation for which repolarizing K^+ currents should be responsible. The left column of data in Fig. 3 shows that I_{Kr}, I_{Ks} and I_{K1} channels mediate such currents. In particular, I_{K1} channels were activated soon after T_{min} and mediated very large outward currents (Fig. 3k). Thus, it is likely that activation of I_{Kr} and I_{Ks} channels during phase 2 repolarization led to regenerative activation of I_{K1} channels and thereby complete deactivation of $I_{Ca,L}$ channels during phase 3 repolarization.

However, when I_{Kr} and I_{Ks} channels were blocked (right column in Fig. 3), the repolarization rate around T_{min} was diminished (*dV/dt* at T_{min} was −0.78 and −0.16 *V*/s, Fig. 3a, b), and I_{K1} currents increased ~50 ms after T_{min} (Fig. 3l). This delayed increase in I_{K1} currents delayed deactivation of $I_{Ca,L}$ channels (Fig. 4d) and $I_{Ca,L}$ channels mediated inward currents for a longer time after T_{min} in the presence of the blockers (Fig. 3f).

L-Type Ca^{2+} and K^+ Currents During Action Potentials with EADs

In order to evaluate $I_{Ca,L}$ and K^+ currents during action potentials which showed EADs, we used the two exemplar

action potentials shown in Fig. 5 as action potential-clamp stimuli. That shown in Fig. 5a was recorded from a myocyte treated with 10 μM E4031 and 20 μM 293B. This action potential had an EAD with a take-off potential of ~ -6 mV and an amplitude of ~ 7 mV. That shown in Fig. 5b was recorded from a different myocyte, which had been treated with 10 μM E4031 and 50 μM 293B. In this case, EADs could not be clearly separated from the preceding action potential due to a depolarized take-off potential and a diminished amplitude.

The black traces in Fig. 5c, d were total membrane currents recorded under the control condition, while gray traces indicate those in the presence of 10 μM E4031 and 20 μM 293B (Fig. 5c) or 10 μM E4031 and 50 μM 293B (Fig. 5d). In both cases, total membrane currents were outward and fluctuated before abruptly increasing and then decreasing at the end of the EADs. In the left-hand column of Fig. 5, $I_{Ca,L}$ channels mediated an inward current throughout the action potential and the EAD (Fig. 5e). $I_{Ca,L}$ currents did not decay smoothly but exhibited a small notch (arrow) on the upstroke of the EAD. I_{Kr} currents in Fig. 5g were recorded in the control condition but should have been absent when the action potential (Fig. 5a) was recorded in the presence of 10 μM E4031. The black trace in Fig. 5i indicates an I_{Ks} current in the control condition, while the gray trace indicates current in the presence of 20 μM 293B. The latter transiently increased during phase 2 of the action potential and stayed almost constant throughout the EAD. I_{K1} currents slightly increased before the EAD took off (arrowhead) and abruptly increased when the EAD terminated (Fig. 5k).

In the right-hand column of Fig. 5, $I_{Ca,L}$ channels again mediated an inward current throughout the action potential and EADs (Fig. 5f). In this case, $I_{Ca,L}$ currents decayed smoothly and did not show discernable notches. I_{Kr} and I_{Ks} currents shown in Fig. 5h, j were recorded under the control condition but should have been absent when the action potential (Fig. 5b) was recorded in the presence of 10 μM E4031 and 50 μM 293B. I_{K1} channels mediated an almost constant outward current throughout the action potential and EADs and a large transient outward current at the end of the EADs (Fig. 5l). Together these results suggest that $I_{Ca,L}$ and I_{K1} channels play pivotal roles in the genesis and termination of EADs.

The Kinetics of L-Type Ca^{2+} Channels During Action Potentials with EADs

The activation, inactivation and recovery of $I_{Ca,L}$ channels during action potentials with EADs are shown in Fig. 6. In the left-hand column, d_{AP} transiently decreased to 0.82 before the EAD took off and then increased to 0.95 during the upstroke of the EAD (Fig. 6c). Thereafter, d_{AP} gradually decreased before promptly declining to zero at the end of the EAD. f_{AP} decreased during phase 2 of the action potential but slightly and significantly increased just before the EAD took off (Fig. 6c). Thereafter, f_{AP} decreased to a minimum of 0.019 at 933 ms. f_{AP_V} almost monotonously decreased until the end of the EAD, and it did not exhibit a clear notch before the EAD took off (Fig. 6c). f_{AP_Ca} decreased during the action potential and showed a small notch before the EAD took off (Fig. 6e). Thus, $I_{Ca,L}$ channels were partially deactivated and modestly recovered from Ca^{2+}-induced inactivation as the EAD took off. In the upstroke of the EAD, $I_{Ca,L}$ channels were reactivated and formed the notch of $I_{Ca,L}$ currents (Fig. 5e, arrow). At T_{min}, f_{AP} was small (0.019) but $I_{Ca,L}$ channels still mediated a measurable inward current because d_{AP} and the driving force were relatively large (equation 4, Figs. 5e and 6c). After T_{min}, $I_{Ca,L}$ channels mediated an inward current until it was completely deactivated by I_{K1} currents ~ 190 ms after T_{min} (Figs. 5e, k and 6c).

In Fig. 6d, d_{AP} gradually decreased throughout the action potential before rapidly declining at the end of the EAD. f_{AP} decreased monotonously to a minimum of 0.023 at 1,157 ms and increased slightly at the end of the EAD. f_{AP_V} and f_{AP_Ca} also decreased during the action potential before increasing slightly at the end of the EAD (Fig. 6d, f).

Fig. 3 Total membrane, L-type Ca^{2+} and K^+ currents flowing during ▶ action potential clamp. (**a, b**) Action potentials used for action potential-clamp experiments with APD_{90} of 396 and 606 ms, respectively. Action potential stimuli were applied to myocytes at 0.33 Hz. (**a**) Control conditions. The action potential in (**b**) was recorded in the presence of 10 μM E4031 and 10 μM 293B. (**c–l**) Time-dependent changes in the total myocyte current density (I_{total}) (**c, d**) and the current density of $I_{Ca,L}$ (**e, f**), I_{Kr} (**g, h**), I_{Ks} (**i, j**) and I_{K1} channels (**k, l**). In the experiments shown in the *left column*, Cd^{2+} (100 μM) plus nifedipine (10 μM), E4031 (10 μM), 293B (50 μM) and Ba^{2+} (2 mM) were sequentially added to myocytes in this order. First, I_{total} was measured in the absence of the drugs. Then, $I_{Ca,L}$, I_{Kr}, I_{Ks} and I_{K1} were measured as a part of the membrane current density inhibited by Cd^{2+} plus nifedipine, E4031, 293B and Ba^{2+}, respectively. In the experiments shown in the *right column*, Cd^{2+} (100 μM) plus nifedipine (10 μM), E4031 (10 μM), 293B (10 μM), 293B (50 μM) and Ba^{2+} (2 mM) were sequentially added to myocytes in this order. I_{total}, $I_{Ca,L}$, I_{Kr} and I_{K1} were measured as above. The *black* I_{Ks} *trace* in **j** was measured as a 293B (50 μM)-sensitive difference current density ($I_{Ks\text{-}total}$). The *gray* I_{Ks} *trace* in **j** was measured as a difference between a current density before addition of 293B (50 μM; i.e., in the presence of 293B [10 μM]) and that after addition of 293B (50 μM) and represents I_{Ks} in the presence of 293B (10 μM) (I_{Ks-10}). The *black* I_{total} *trace* in **d** was measured as above, while the *gray trace* was calculated as $I_{total} - I_{Kr} - I_{Ks\text{-}total} + I_{Ks-10}$ and represents a total membrane current density in the presence of E4031 (10 μM) and 293B (10 μM). Note that I_{total} contains $I_{Ca,L}$, I_{Kr}, I_{Ks} and I_{K1} and background currents. Each current trace is the mean of five stimuli. *Horizontal lines* indicate the zero potential (**a, b**) or current (**c–l**) level. *Vertical dotted lines* indicate the time of minimum $I_{Ca,L}$ availability (T_{min}) (*left* 368 ms, *right* 506 ms) (see Fig. 4)

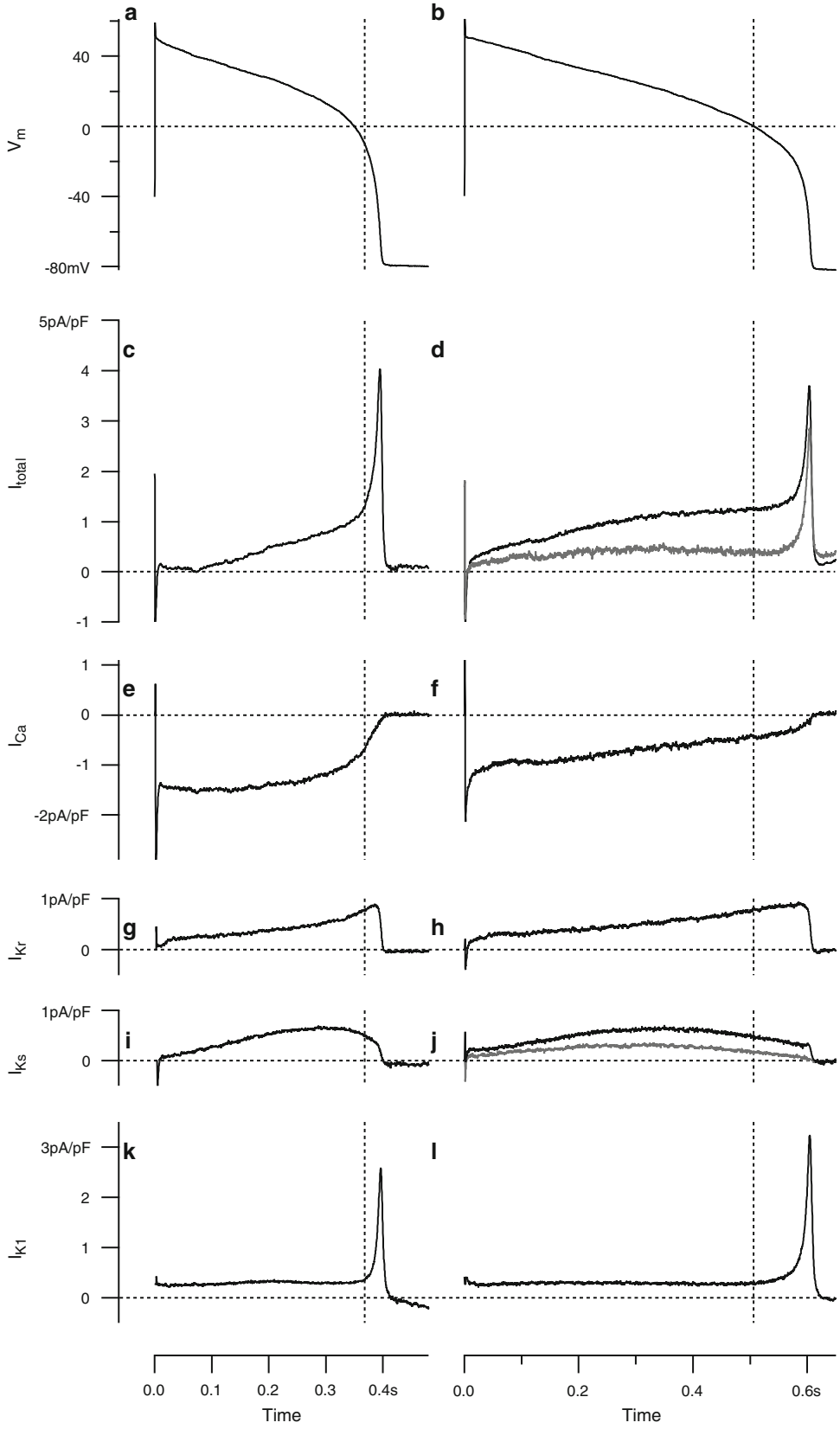
a
b
40
0
-40
-80mV
V_m
5pA/pF
c
d
4
3
2
1
0
-1
I_{total}
1
e
f
0
-1
-2pA/pF
I_{Ca}
1pA/pF
g
h
0
I_{Kr}
1pA/pF
i
j
0
I_{Ks}
3pA/pF
k
l
2
1
0
I_{K1}
0.0
0.1
0.2
0.3
0.4s
Time
0.0
0.2
0.4
0.6s
Time

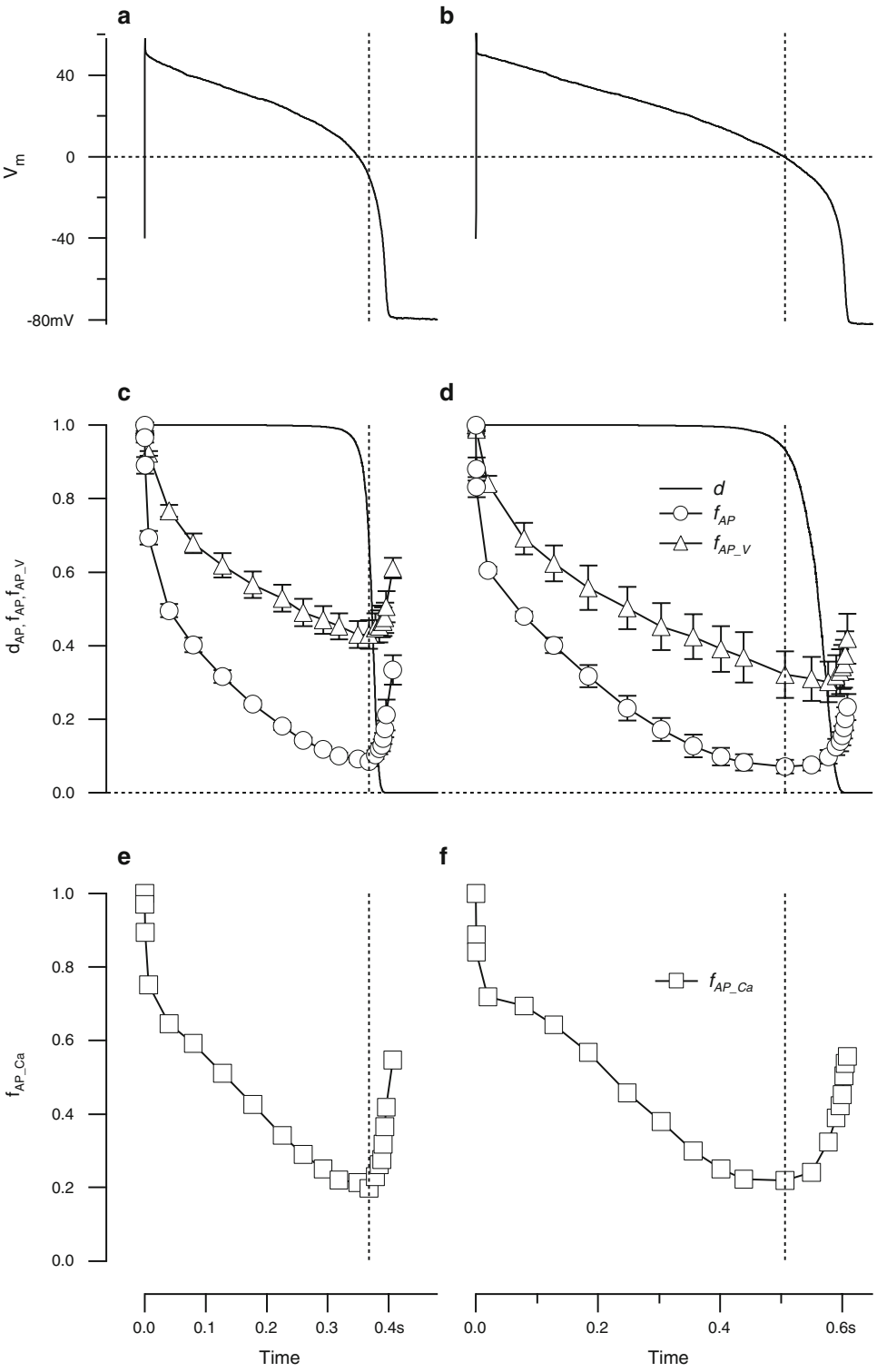

Fig. 4 The kinetics of L-type Ca^{2+} channels during action potential clamp. (**a, b**) The same representative action potentials shown in Fig. 3. (**c, d**) Activation and inactivation of I_{CaL} channels in action potentials. Inactivation in action potentials was assessed with the gapped double pulse action potential clamp protocol. The action potential was interrupted when the membrane potential was +59, +54, +52, +50, +45, +40, +35, +30, +25, +20, +15, +10, 0, −10, −20, −30, −40, −50, −60, −70 m*V* and the resting membrane potential (−79 m*V*) in the *left column* and +61, +53, +52, +50, +45, +40, +35, +30, +25, +20, +15, +10, 0, −10, −20, −30, −40, −50, −60, −70 m*V* and the resting membrane potential (−79 m*V*) in the *right column*. *Continuous lines* represent activation in action potentials (d_{AP}). Symbols represent inactivation in action potentials in the presence of Ca^{2+} (○, f_{AP}) or Ba^{2+} (△, f_{AP_V}). (**e, f**) The Ca^{2+}-dependent component of inactivation in action potentials (□, f_{AP_Ca}) estimated from f_{AP} and f_{AP_V} with eq. 3. Symbols and bars represent mean and SE ($n = 5$ for each point). *Vertical dotted lines* indicate T_{min}

Again, $I_{Ca,L}$ channels mediated a measurable inward current at T_{min} in spite of the small f_{AP} (Fig. 5f). This current was eventually eliminated by deactivation induced by delayed activation of I_{K1} channels ∼300 ms after T_{min} (Figs. 5f, l and 6d).

Taken together, these results indicate that the common mechanism underlying these two types of EAD is the failure of complete deactivation of $I_{Ca,L}$ channels and the resultant sustained inward current at the end of phase 2 repolarization.

Discussion

Inward Currents Induce EADs when Delayed Rectifier K^+ Currents Are Blocked

E4031 and 293B evoked EADs when applied in combination to isolated guinea pig ventricular myocytes (Fig. 1). When both I_{Kr} and I_{Ks} channels were completely blocked, EADs were not clearly separated from the preceding action potentials. This type of EAD would have the same pathophysiological effects on myocardial electrical activity as the prototypical phase 2 EADs such as conduction block and "prolonged repolarization-dependent reexcitation" (Brugada and Wellens 1985).

A selective $I_{Ca,L}$ blocker, nifedipine, more potently shortened action potentials with EADs than those without EADs (Fig. 2). Thus, an $I_{Ca,L}$ current is critically involved in EADs caused by suppression of I_{Kr} and I_{Ks} currents (Marbán et al. 1986; Zeng and Rudy 1995; Anderson et al. 1998). The Na–Ca exchanger blocker SEA0400 had a lesser inhibitory effect on EADs than nifedipine under this condition.

Mechanism Underlying EADs

January and Riddle (1989) analyzed EADs induced by the $I_{Ca,L}$ channel agonist BayK8644 in sheep Purkinje fibers and concluded that $I_{Ca,L}$ channels recovered before EADs and generated EADs. The EADs they found took off at ~ -30 mV and had an amplitude of up to ~ 40 mV. They also showed that the amplitude of EADs was inversely correlated with the take-off potential of EADs, indicating that the recovery of $I_{Ca,L}$ channels before EADs is strongly dependent on the take-off potential. When I_{Kr} and I_{Ks} channels were suppressed, EADs took off at more depolarized potentials (~ -10 to 0 mV) and had a much smaller amplitude (<15 mV) than January and Riddle (1989) found (Fig. 1). Under this condition, $I_{Ca,L}$ channels recovered only modestly, if at all, before EADs took off (Fig. 6c, d).

A theoretical study indicated that the recovery and reactivation of $I_{Ca,L}$ channels also caused EADs when K^+ currents were suppressed (Zeng and Rudy 1995). In this model, f_{AP_Ca} rapidly reaches a minimum of ~ 0.1 during the initial ~ 10 ms and then increases to ~ 0.5 before EADs take off. Thus, Ca^{2+}-dependent inactivation proceeds very rapidly and reverses substantially. The authors reasoned that when action potentials were longer, $I_{Ca,L}$ channels recovered further from Ca^{2+}-dependent inactivation during action potentials and thereby induced EADs. However, f_{AP_Ca} in the model was a pure function of intracellular Ca^{2+} concentration and thus mirrors a simulated intracellular Ca^{2+} transient (Luo and Rudy 1994). These predictions differ from our experimental results (Figs. 4c, d and 6c, d), where $I_{Ca,L}$ channels did not recover during action potentials either as promptly or as substantially as suggested by the model.

We found that in action potentials the decay of $I_{Ca,L}$ currents after T_{min} resulted from deactivation, in which the regenerative activation of I_{K1} currents soon after T_{min} played a particularly important role (Figs. 3k and 4c, d) (Luo and Rudy 1994; Linz and Myer 1998a, 2000). When I_{Kr} and I_{Ks} channels were blocked, activation of I_{K1} channels and complete deactivation of $I_{Ca,L}$ channels did not occur so soon after T_{min} (Figs. 3f, l and 4d). We speculate that this more sustained $I_{Ca,L}$ current after T_{min} contributes to the genesis of EADs by block of I_{Kr} and I_{Ks} channels (Fig. 3f).

We analyzed two types of action potentials with EADs (Fig. 5a, b). In both cases, there were sustained $I_{Ca,L}$ currents during EADs until they were completely deactivated by I_{K1} currents at the end of EADs (Figs. 5e, f, k, l and 6c, d). These results suggest that the essential mechanism underlying EADs is the failure of complete deactivation of $I_{Ca,L}$ channels when I_{Kr} and I_{Ks} channels are suppressed. Depending on the extent of repolarization before EADs take off, $I_{Ca,L}$ channels can recover from Ca^{2+}-dependent inactivation and subsequent regenerative activation of $I_{Ca,L}$ channels would create the upstroke of EADs (Figs. 5e and 6c). However, this phenomenon was modest, if it occurred at all, and did not seem to be essential for EADs when I_{Kr} and I_{Ks} currents were suppressed. Submicromolar nifedipine effectively suppressed EADs (Fig. 2), probably because it partially reduced $I_{Ca,L}$ currents at the end of the phase 2 repolarization and allowed activation of I_{K1} channels and complete deactivation of $I_{Ca,L}$ channels.

Ca^{2+}-induced facilitation of $I_{Ca,L}$ channels may be involved in the genesis of EADs (Wu et al. 1999). The prolonged Ca^{2+} transient associated with prolonged action potentials may increase $I_{Ca,L}$ currents by activating calmodulin-dependent kinase. However, we did not see clear Ca^{2+}-induced facilitation when action potentials with EADs were applied to myocytes, nor did we find larger $I_{Ca,L}$ currents in longer action potentials (Figs. 3e, f and 5e, f).

Clinical Implications

That nifedipine more potently shortened action potentials with EADs than without EADs in clinical blood concentrations (<1 μM) (Fig. 2) indicates that nifedipine may not only suppress the trigger of the arrhythmias but also reduce the dispersion of refractoriness in LQT patients. Verapamil, a phenylalkylamine Ca^{2+} channel blocker, has been reported to be effective at suppressing epinephrine-induced EADs in familial LQT patients (Shimizu et al. 1995). Its mode of action may be the same as that shown for nifedipine in this study.

β-Blocking agents are currently the major therapy for familial LQT patients when the genotype cannot be identified (Schwartz 2005). This probably indicates that β-adrenergic stimulation increases $I_{Ca,L}$ currents and the incidence of EADs. Because nifedipine and β-blocking agents are safely used in combination for many cardiovascular diseases (Hoffman 2006; Michel 2006), nifedipine (and probably other dihydropyridines) can be a drug of choice for treatment of LQT patients with reduced delayed rectifier K^+ currents.

Limitation of Present Study

In ideal conditions of action potential-clamp experiments, each action potential stimulus should be derived from an action potential recorded in the same myocyte. To measure action potentials and f_{AP} in the same myocyte, it is necessary to automatically and promptly determine at which time and potential action potentials should be interrupted to adequately assess f_{AP} within a span of a single patch-clamp experiment. However, this is usually difficult and requires fine manual adjustment, especially in action potentials associated with EADs in which membrane potential changed slowly or passed the same value more than once. Thus, we analyzed the averages of the kinetics of $I_{Ca,L}$ channels in exemplar action potentials and compared them with averaged channel currents in the exemplar action potentials as done by Linz and Myer (1998a).

We included 100 μM EGTA in the pipette solution, which would have modified the amplitude and kinetics of $I_{Ca,L}$ currents. However, it should be noted that the peak $I_{Ca,L}$ current density measured in this study was comparable with that measured without Ca^{2+} buffers (Doerr et al. 1990; Linz and Meyer 1998a, 2000) but much smaller than that measured with strong Ca^{2+} buffers in pipette solutions (Arreola et al. 1991; Grantham and Cannell 1996). We assessed f_{AP_V} by using Ba^{2+} as a permeant. However, Ba^{2+}-mediated $I_{Ca,L}$ currents inactivate slightly faster and to a larger extent than Na^+-mediated ones in a range of action potentials (Findlay 2002). Thus, we might have overestimated f_{AP_V}.

Cd^{2+} used to block $I_{Ca,L}$ currents modulates I_{Kr} and I_{Ks} currents in a voltage-dependent manner (Daleau et al. 1997). Thus, I_{Kr} and I_{Ks} currents measured in the presence of Cd^{2+} might have been over- or underestimated by up to 30% depending on the membrane potential. The effect of Cd^{2+} on these K^+ currents also might have caused an error in the measurement of f_{AP}. However, f_{AP} assessed when intra- and extracellular K^+ was completely replaced with Cs^+ and tetraethylammonium to block all K^+ currents was not significantly different from that shown in Figs. 4 and 6. Cd^{2+} and Ba^{2+} also block $I_{Na\text{-}Ca}$ currents (Blaustein and Lederer 1999). However, isolated $I_{Ca,L}$ and I_{K1} currents were not apparently contaminated with $I_{Na\text{-}Ca}$ currents, which are inward and as large as peak $I_{Ca,L}$ currents near the end of action potentials (Figs. 3 and 5) (Armoundas et al. 2003).

During records, channel currents ran down. In experiments shown in Figs. 3 and 5, Cd^{2+} plus nifedipine, E4031, 293B and Ba^{2+} were, respectively, applied at 85 ± 3, 162 ± 6, 256 ± 9 and 341 ± 14 s after formation of the whole-cell configuration. At these times, $I_{Ca,L}$, I_{Kr}, I_{Ks} and I_{K1} currents ran down to 99.6 ± 4.6%, 94.8 ± 14.8%, 92.7 ± 6.3% and 91.5 ± 5.0%, respectively.

The 200-ms prepulse to −40 m*V* might have affected the measurement of membrane currents, d_∞ and f_{AP}. Thus, we measured a total membrane current and f_{AP} in action potentials preceded by a 10-ms prepulse to −40 m*V*. The measured total membrane currents were not significantly different from those shown in Figs. 3 and 5. f_{AP} measured with a 10-ms prepulse was slightly but significantly higher than that measured with a 200-ms prepulse throughout an action potential. However, T_{min} was the same irrespective of the prepulse durations. Finally, $V_{0.5}$ and k determining d_∞ (equation 2) were measured in rectangular voltage pulses preceded by a 10- or 200-ms prepulse to −40 m*V*.

Fig. 5 L-type Ca^{2+} and K^+ currents flowixng during action potential▶ stimuli showing EADs. (**a, b**) Action potentials used for action potential-clamp experiments. The action potentials were recorded from two different myocytes paced at 0.33 Hz in the presence of 10 μM E4031 and 20 μM 293B (**a**) or 10 μM E4031 and 50 μM 293B (**b**). **c–l** Time-dependent changes in the total myocyte current density (**c, d**) and the current density of $I_{Ca,L}$ (**e, f**), I_{Kr} (**g, h**), I_{Ks} (**i, j**) and I_{K1} channels (**k, l**). In the experiments shown in the *left column*, Cd^{2+} (100 μM) plus nifedipine (10 μM), E4031 (10 μM), 293B (20 μM), 293B (50 μM) and Ba^{2+} (2 mM) were sequentially added to myocytes in this order. First, I_{total} was measured in the absence of the drugs (*black trace* in **c**). Then, $I_{Ca,L}$, I_{Kr} and I_{K1} were measured as a part of the membrane current density inhibited by Cd^{2+} plus nifedipine, E4031 and Ba^{2+}, respectively. The *black* I_{Ks} *trace* in (**i**) was measured as a 293B (50 μM)-sensitive difference current density ($I_{Ks\text{-}total}$). The gray I_{Ks} trace in (**i**) was measured as a difference between current density before addition of 293B (50 μM; i.e., in the presence of 293B [20 μM]) and that after addition of 293B (50 μM) and represents I_{Ks} in the presence of 293B (20 μM) (I_{Ks-20}). The *gray* I_{total} *trace* in (**c**) was calculated as $I_{total} - I_{Kr} - I_{Ks\text{-}total} + I_{Ks-20}$ and represents a total membrane current density in the presence of E4031 (10 μM) and 293B (20 μM). In the experiments shown in the *right column*, Cd^{2+} (100 μM) plus nifedipine (10 μM), E4031 (10 μM), 293B (50 μM) and Ba^{2+} (2 mM) were sequentially added to myocytes in this order. First, I_{total} was measured in the absence of the drugs (*black trace* in **d**). Then, $I_{Ca,L}$, I_{Kr}, I_{Ks} and I_{K1} were measured as a part of the membrane current density inhibited by Cd^{2+} plus nifedipine, E4031, 293B and Ba^{2+}, respectively. The *gray* I_{total} *trace* in (**d**) was calculated as $I_{total} - I_{Kr} - I_{Ks}$ and represents a total membrane current density in the presence of E4031 (10 μM) and 293B (50 μM). Note that I_{total} contains $I_{Ca,L}$, I_{Kr}, I_{Ks}, I_{K1} and background currents. Each current trace is the mean of five stimuli. *Arrow* in (**e**) indicates a notch in $I_{Ca,L}$ currents observed on the upstroke of the EAD. *Arrowhead* in (**k**) indicates partial activation of I_{K1} channels before the EAD took off. *Vertical dotted lines* indicate T_{min} (*left* 933 ms, *right* 1,158 ms)

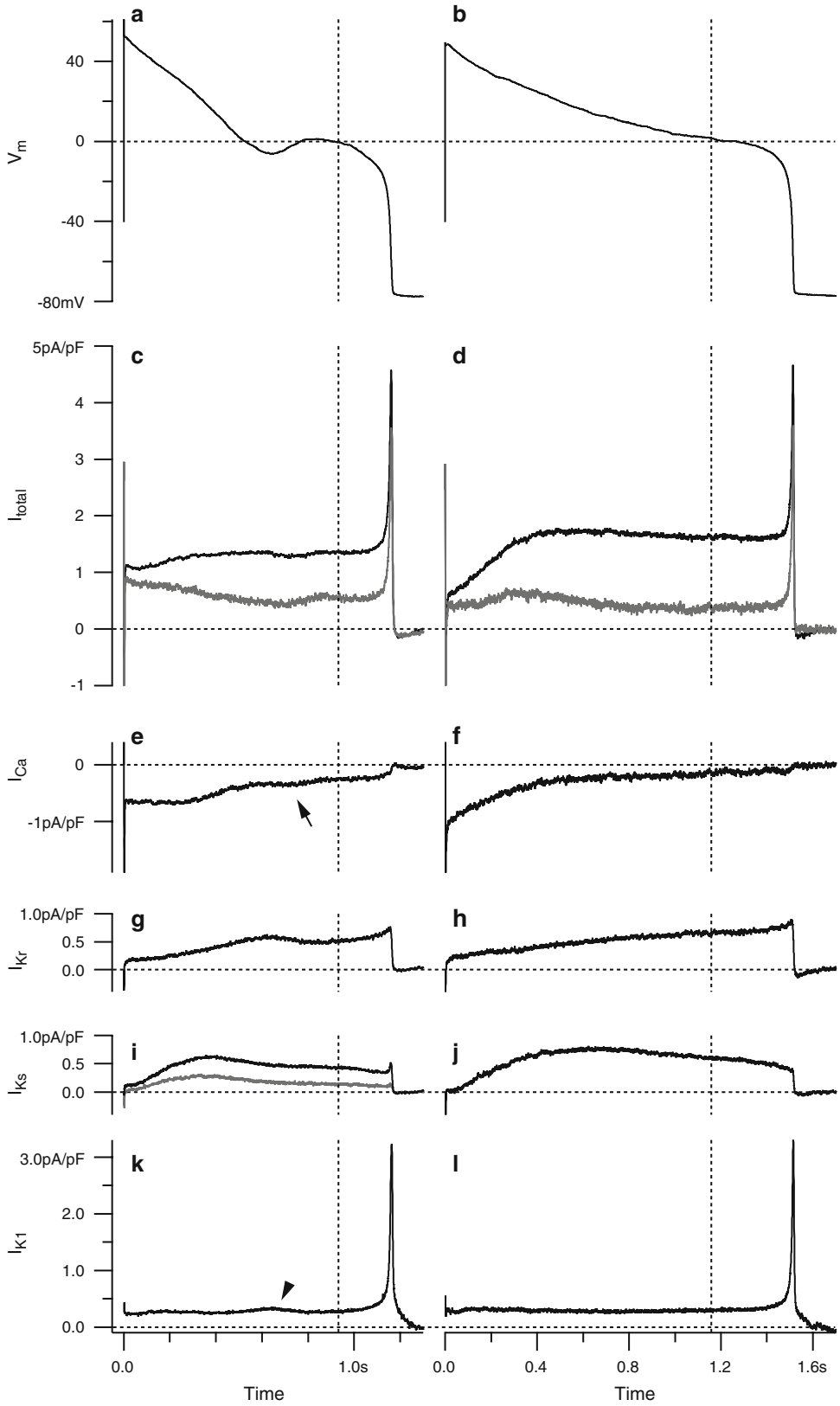
a
b
40
0
-40
-80mV
V_m
5pA/pF
c
d
4
3
2
1
0
-1
I_{total}
e
f
0
-1pA/pF
I_{Ca}
1.0pA/pF
g
h
0.5
0.0
I_{Kr}
1.0pA/pF
i
j
0.5
0.0
I_{Ks}
3.0pA/pF
k
l
2.0
1.0
0.0
I_{K1}
0.0
1.0s
Time
0.0
0.4
0.8
1.2
1.6s
Time

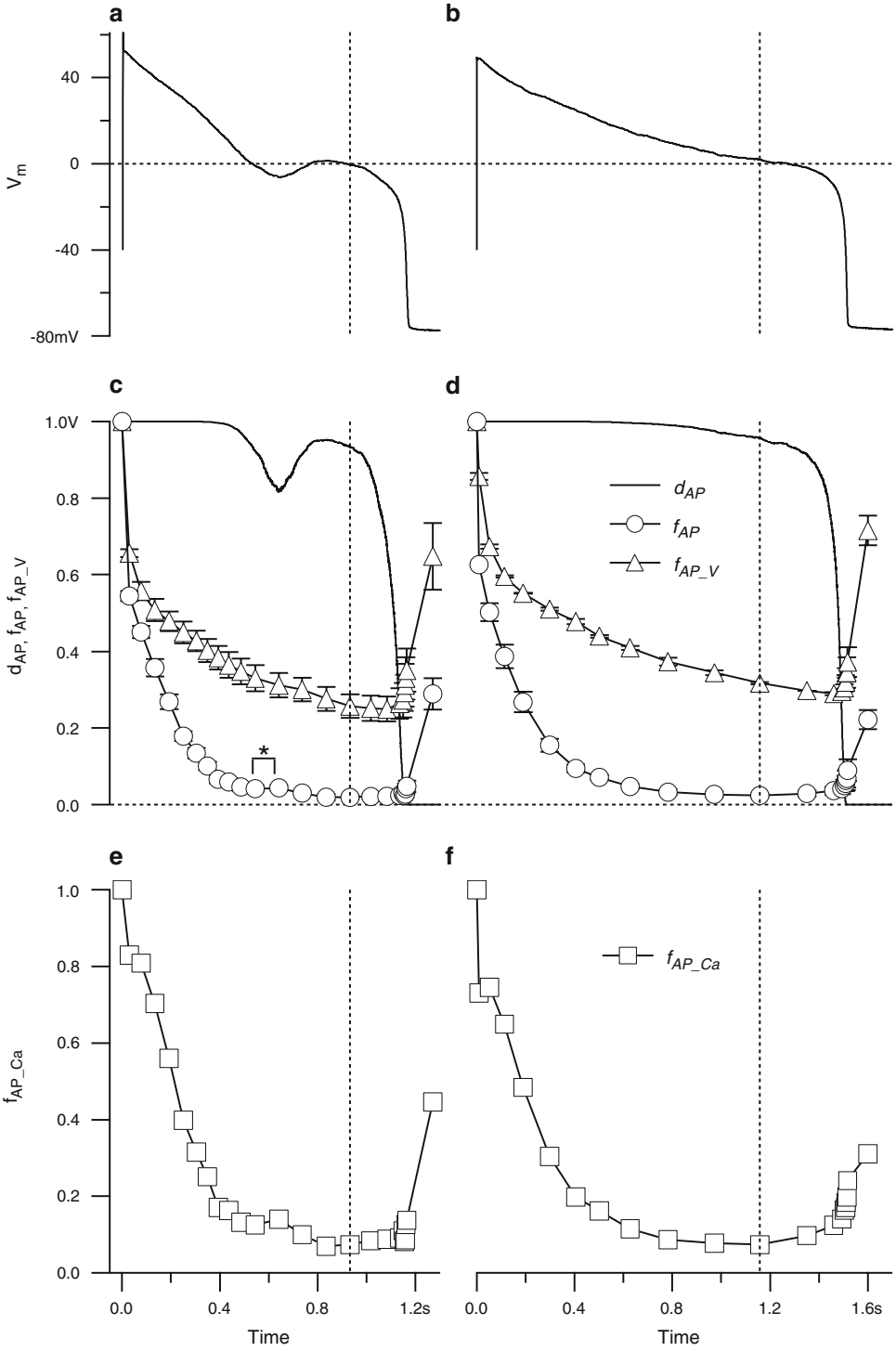

Fig. 6 The kinetics of L-type Ca^{2+} channels during action potential stimuli showing EADs. (**a**, **b**) The same representative action potentials shown in Fig. 5. (**c**, **d**) Activation and inactivation of I_{CaL} channels in action potentials. Inactivation in action potentials was assessed with the gapped double pulse action potential clamp protocol. The action potential was interrupted when the membrane potential was +61, +50, +45, +40, +35, +30, +25, +20, +15, +10, +4, −1, −6, −2, +1, 0, −4, −10, −20, −30, −40, −50, −60, −70 and the resting membrane potential (−77 m*V*) and +50, +49, +45, +40, +35, +30, +25, +20, +15, +10, +5, +2, −2, −10, −20, −30, −40, −50, −60, −70 and the resting membrane potential (−77 m*V*). *Continuous lines* indicate activation in action potentials (d_{AP}). Symbols represent inactivation in action potentials in the presence of Ca^{2+} (○, f_{AP}) or Ba^{2+} (△, f_{AP_V}). (**e, f**) The Ca^{2+}-dependent component of inactivation in action potentials (□, f_{AP_Ca}) was estimated from f_{AP} and f_{AP_V} with equation 3. Symbols and bars represent mean and SE ($n = 5$ for each point). *Vertical dotted lines* indicate T_{min}. *Statistically significant difference ($P < 0.05$) as judged by Student's paired *t*-test

They were not significantly affected by the prepulse durations.

Acknowledgments We are grateful to Dr. Ian Findlay (Centre National de la Recherche Scientifique UMR 6542, Faculté des Sciences, Université François Rabelais de Tours, France) for critical reading of this manuscript and Ms. Reiko Sakai for secretarial assistance.

References

Alseikhan BA, DeMaria CD, Colecraft HM, Yue DT (2002) Engineered calmodulins reveal the unexpected eminence of Ca^{2+} channel inactivation in controlling heart excitation. Proc Natl Acad Sci USA 99:17185–17190

Anderson ME, Braun AP, Wu Y, Lu T, Wu Y, Schulman H, Sung RJ (1998) KN-93, an inhibitor of multifunctional Ca^{++}/calmodulin-

dependent protein kinase, decreases early afterdepolarizations in rabbit heart. J Pharmacol Exp Ther 287:996–1006

Antzelevitch C, Shimizu W (2002) Cellular mechanisms underlying the long QT syndrome. Curr Opin Cardiol 17:43–51

Armoundas AA, Hobai IA, Tomaselli GF, Winslow RL, O'Rourke B (2003) Role of sodium–calcium exchanger in modulating the action potential of ventricular myocytes from normal and failing hearts. Circ Res 93:46–53

Arreola J, Dirksen RT, Shieh R-C, Williford DJ, Sheu S (1991) Ca^{2+} currents and Ca^{2+} transients under action potential clamp in guinea pig ventricular myocytes. Am J Physiol 261:C393–C397

Birinyi P, Aesai K, Bányász T, Tóth A, Horváth B, Virág L, Szentandrássy N, Magyar J, Varró A, Fülöp F, Nánási PP (2005) Effects of SEA0400 and KB-R7943 on Na^+/Ca^{2+} exchange current and L-type Ca^{2+} current in canine ventricular cardiomyocytes. Naunyn-Schmiedebergs Arch Pharmacol 372:63–70

Blaustein MP, Lederer WJ (1999) Sodium/calcium exchange: its physiological implications. Physiol Rev 79:763–854

Bosch RF, Gaspo R, Busch AE, Lang HJ, Li G-R, Nattel S (1998) Effects of the chromanol 293B, a selective blocker of the slow, component of the delayed rectifier K^+ current, on repolarization in human and guinea pig ventricular myocytes. Cardiovasc Res 38:441–450

Brugada P, Wellens HJJ (1985) Early afterdepolarizations: role in conduction block, "prolonged repolarization-dependent reexcitation," and tachyarrhythmia in the human heart. Pace 8:889–896

Cranefield PF, Aronson RS (1988) The causes, characteristics, and consequences of early afterdepolarizations. In: Cranefield PF, Aronson RS (eds) Cardiac arrhythmias: the role of triggered activity and other mechanisms. Futura, New York, pp 431–479

Daleau P, Khalifa M, Turgeon J (1997) Effects of cadmium and nisoldipine on the delayed rectifier potassium current in guinea pig ventricular myocytes. J Pharmacol Exp Ther 281:826–833

Damiano BP, Rose MR (1984) Effects of pacing on triggered activity induced by early afterdepolarizations. Circulation 5:1013–1025

Doerr T, Denger R, Doerr A, Trautwein W (1990) Ionic currents contributing to the action potential in single ventricular myocytes of the guinea pig studied with action potential clamp. Pfluegers Arch 416:230–237

Fabiato A (1985) Simulated calcium current can both cause calcium loading in and trigger calcium release from the sarcoplasmic reticulum of a skinned canine cardiac Purkinje cell. J Gen Physiol 85:291–320

Findlay I (2002) Voltage- and cation-dependent inactivation of L-type Ca^{2+} channel currents in guinea pig ventricular myocytes. J Physiol 541:731–740

Grantham CJ, Cannell MB (1996) Ca^{2+} influx during the cardiac action potential in guinea pig ventricular myocytes. Circ Res 79:194–200

Hamill OP, Marty A, Neher E, Sakmann B, Sigworth FJ (1981) Improved patch-clamp techniques for high-resolution current recording from cells and cell-free membrane patches. Pfluegers Arch 391:85–100

Hardley RW, Lederer WJ (1991) Ca^{2+} and voltage inactivate Ca^{2+} channels in guinea pig ventricular myocytes through independent mechanisms. J Physiol 444:257–268

Hoffman BB (2006) Therapy of hypertension. In: Brunton LL (ed) The pharmacological basis of therapeutics, 11th edn. McGraw-Hill, New York, pp 845–868

January CT, Riddle JM (1989) Early afterdepolarizations: mechanism of induction and block. A role for L-type Ca^{2+} current. Circ Res 64:977–990

Kass RS, Sanguinetti MC (1984) Inactivation of calcium channel current in the calf cardiac Purkinje fiber. Evidence for voltage- and calcium-mediated mechanisms. J Gen Physiol 84:705–726

Keating MT, Sanguinetti MC (2001) Molecular and cellular mechanisms of cardiac arrhythmias. Cell 104:569–580

Lee KS, Marbán E, Tsien RW (1985) Inactivation of calcium channels in mammalian heart cells: joint dependence on membrane potential and intracellular calcium. J Physiol 364:395–411

Linz KW, Myer R (1998a) Control of L-type calcium current during the action potential of guinea pig ventricular myocytes. J Physiol 513:425–442

Linz KW, Myer R (1998b) The late component of L-type calcium current during guinea pig cardiac action potentials and its contribution to contraction. Pfluegers Arch 436:679–688

Linz KW, Myer R (2000) Profile and kinetics of L-type calcium current during the cardiac ventricular action potential compared in guinea pigs, rats and rabbits. Pfluegers Arch 439:588–599

Luo C-H, Rudy Y (1994) A dynamic model of the cardiac ventricular action potential. I Simulations of ionic currents and concentration changes. Circ Res 74:1071–1096

Marbán E, Robinson SW, Wier WG (1986) Mechanisms of arrhythmogenic delayed and early afterdepolarizations in ferret ventricular muscle. J Clin Invest 78:1185–1192

Matsuda T, Arakawa N, Takuma K, Kishida Y, Kawasaki Y, Sakaue M, Takahashi K, Takahashi T, Suzuki T, Ota T, Hamano-Takahashi A, Onishi M, Tanaka Y, Kameo K, Baba A (2001) SEA0400, a novel and selective inhibitor of the Na^+–Ca^{2+} exchanger, attenuates reperfusion injury in the in vitro and in vivo cerebral ischemic models. J Pharmacol Exp Ther 298:249–256

McDonald TF, Pelzer S, Trautwein W, Pelzer DJ (1994) Regulation and modulation of calcium channels in cardiac, skeletal, and smooth muscle cells. Physiol Rev 74:365–507

Michel T (2006) Treatment of myocardial ischemia. In: Brunton LL (ed) The pharmacological basis of therapeutics, 11th edn. McGraw-Hill, New York, pp 823–844

Nagy ZA, Virág L, Tóth A, Biliczki P, Acsai K, Bányász T, Nánási P, Papp JG, Varró A (2004) Selective inhibition of sodium–calcium exchanger by SEA-0400 decreases early and delayed afterpolarization in canine heart. Br J Pharmacol 143:827–831

Priori SG, Corr PB (1990) Mechanisms underlying early and delayed afterpolarizations induced by catecholamines. Am J Physiol 27:H1796–H1805

Sanguinetti MC, Jurkiewicz NK (1990) Two components of cardiac delayed rectifier K^+ current. Differential sensitivity to block by class III antiarrhythmic agents. J Gen Physiol 96:195–215

Schwartz PJ (2005) Management of long QT syndrome. Nat Clin Pract Cardiovasc Med 2:346–351

Shimizu W, Ohe T, Kurita T, Kawade M, Arakaki Y, Aihara N, Kamakura S, Kamiya T, Shimomura K (1995) Effects of verapamil and propranolol on early afterdepolarizations and ventricular arrhythmias induced by epinephrine in congenital long QT syndrome. J Am Coll Cardiol 26:1299–1309

Shirokov R, Levis R, Shirokova N, Ríos E (1993) Ca^{2+}-dependent inactivation of cardiac L-type Ca^{2+} channels does not affect their voltage sensor. J Gen Physiol 102:1005–1030

Sicouri S, Quist M, Antzelevitch C (1996) Evidence for the presence of M cells in the guinea pig ventricle. J Cardiovasc Electrophysiol 7:503–511

Splawski I, Timothy KW, Sharpe LM, Decher N, Kumar P, Bloise R, Napolitano C, Schwartz PJ, Joseph RM, Condouris K, Tager-Flusberg H, Priori SG, Sanguinetti MC, Keating MT (2004) $Ca_v1.2$ calcium channel dysfunction causes a multisystem disorder including arrhythmia and autism. Cell 119:19–31

Wu Y, MacMillan LB, McNeill RB, Colbran RJ, Anderson ME (1999) CaM kinase augments cardiac L-type Ca^{2+} current: a cellular mechanism for long Q-T arrhythmias. Am J Physiol 276:H2168–H2178

Yamada M, Jahangir A, Hosoya Y, Inanobe A, Katada T, Kurachi Y (1993) G_K* and brain $G_{\beta\gamma}$ activate muscarinic K^+ channel through the same mechanism. J Biol Chem 268:24551–24554

Zeng J, Rudy Y (1995) Early afterdepolarizations in cardiac myocytes: mechanism and rate dependence. Biophys J 68:949–964